Droplets pinned at chemically inhomogenous substrates:
A simulation study of the two-dimensional Ising case

Marta L. Trobo

*Instituto de Física de Líquidos y Sistemas Biológicos (IFLYSIB), CCT-CONICET La Plata, UNLP, Calle 59 Nro. 789, (1900) La Plata,
Argentina and Departamento de Ciencias Básicas, Facultad de Ingeniería, Universidad Nacional de La Plata, Argentina*

Ezequiel V. Albano

*Instituto de Física de Líquidos y Sistemas Biológicos (IFLYSIB), CCT-CONICET La Plata, UNLP, Calle 59 Nro. 789, (1900) La Plata,
Argentina, and Departamento de Física, Facultad de Ciencias Exactas, Universidad Nacional de La Plata, Argentina*

Kurt Binder

Institut für Physik, Johannes Gutenberg-Universität Mainz, Staudinger Weg 7, D-55099 Mainz, Germany

As a simplified model of a liquid nanostripe adsorbed on a chemically structured substrate surface, a two-dimensional Ising system with two boundaries at which surface fields act is studied. At the upper boundary, the surface field is uniformly negative, while at the lower boundary (a distance L apart), the surface field is negative only outside a range of extension b, where a positive surface stabilizes a droplet of the phase with positive magnetization for temperatures T exceeding the critical temperature T_w of the wetting transition of this model. We investigate the local order parameter profiles across the droplet, both in the directions parallel and perpendicular to the substrate, varying both b and T. Also, precursor effects to droplet formation as T approaches T_w from below are studied. In accord with theoretical predictions, for $T > T_w$ the droplet is found to have the shape of a semiellipse, where the width (distance of the interface from the substrate) scale is proportional to b ($b^{1/2}$). So, the area of the droplet is proportional to $b^{3/2}$, and the temperature dependence of the corresponding prefactor, which also involves the interfacial stiffness, is studied.

I. INTRODUCTION

Chemically structured surfaces are of great interest in the context of various applications in nanotechnology, e.g., for the fabrication of nanoscopic electronic devices, the development of efficient processing techniques involving very small amounts of matter ("lab on a chip"), etc. [1]. Nanofluids at structured substrates, however, also pose challenging scientific questions in statistical mechanics [2–5]. There is an interesting interplay between surface effects due to the substrate and interfacial effects due to the liquid-vapor interface of the fluid film (or droplet) adsorbed on the substrate, and due to the considered nanoscopic sizes both statistical fluctuations and systematic finite size effects play an important role. Thus, a chemical inhomogeneity of the substrate, e.g., when the substrate potential discontinuously changes at a "defect line" at the substrate surface, can cause pinning of a fluid-vapor interface along this line, and then the line tension associated with the substrate inhomogeneity matters (e.g., [6–17]). Note, however, that this line tension due to a substrate chemical inhomogeneity should not be confused with the line tension associated with the three-phase contact line where the interface due to a droplet (or liquid ridge) meets a homogeneous substrate (see, e.g., [18–28]).

Progress in statistical physics problems often has been boosted by considering simplified lattice models such as the Ising model. In fact, for the Ising model in $d = 2$ dimensions both the temperature dependence of the bulk order parameter and the interfacial tension are known exactly [29,30], as well as the (critical) wetting transition caused by applying a suitable surface magnetic field H_w at the boundary of a semi-infinite lattice [31,32]. This surface magnetic field represents the potential acting by a solid substrate at the molecules of a fluid, interpreting the Ising system as a lattice gas, the states with positive and negative spontaneous magnetization corresponding to coexisting liquid and vapor phases. For this model, the contact angle of a sessile droplet at a homogeneous substrate can be computed exactly [33], and the character of interfacial fluctuations near the wetting transition is well understood [34], although important facets have only been discovered very recently [35].

The Ising model can also be studied in great detail rather straightforwardly by Monte Carlo simulation [36], and droplets and their fluctuations both in the bulk [37] and attached at a wall [38] have been studied for a long time. However, both recent experimental work [39], where the density profile across liquid nanostripe was measured as a function of strip width and temperatures near the wetting transition temperature, and the availability of exact predictions obtained for a solid-on-solid (SOS) model [40–43] is a motivation to carry out a more complete Monte Carlo study of droplets attached to a nanoscopic chemical inhomogeneity, in the framework of the $d = 2$ Ising model where the surface field takes a positive value along a distance containing b lattice sites (Fig. 1) while everywhere else the surface field is negative. We study the droplet properties here both as a function of temperature across the wetting transition, as in the experiment [39], and of the width b of the chemical heterogeneity of the boundary. In the following section, we briefly summarize the model and the choice of parameters, while in Sec. III we describe our results, and in Sec. IV we summarize our conclusions.
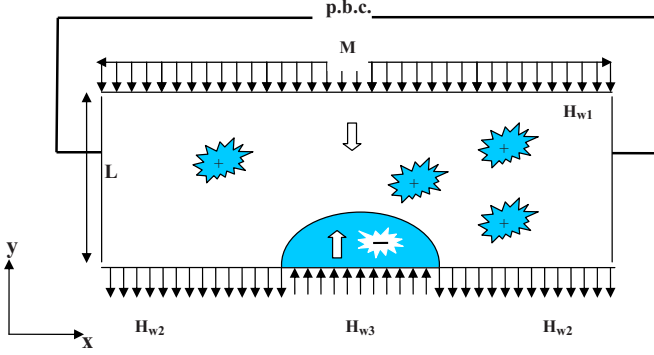
FIG. 1. Schematic description of the system geometry. We choose a rectangular $M \times L$ lattice with periodic boundary conditions in the x direction and surface fields acting on the first and last row of spins in the y direction. The surface field on the top row (H_{w1}) and outside the inhomogeneity at the bottom row (H_{w2}) are both chosen negative, so that a negative magnetization in the bulk of the system is stable, while for b sites at the bottom row a positive field $H_{w3} = |H_{w2}|$ is chosen. The strength H_{w1} of the surface field on top is chosen smaller ($|H_{w1}| = |H_{w2}|/4$), but for the large linear dimensions chosen the precise choice of H_{w1} does not matter with respect to the properties of the droplet.

II. MODEL AND SIMULATION DETAILS

Since we wish to study a system with an inhomogenous boundary field, we write down the Hamiltonian in terms of the two indices (j,i) labeling the lattices sites in (x,y) directions, with $1 \leqslant j \leqslant M$ and $1 \leqslant i \leqslant L$, choosing always the lattice linear dimensions (Fig. 1) L even and M odd, so that the center of the droplet (where its y dimension is largest) is at the lattice site $j = (M + 1)/2$, rather than in between two lattice sites. In the x direction, periodic boundary conditions are applied, while in y direction the rows $i = 1$ and $i = L$ simply have free boundaries but there the spins experience a boundary field. At the upper boundary we choose a field $H_{w1} = -0.225$ to stabilize a domain with negative magnetization. At the lower boundary ($i = 1$) we apply a field $H_{w2} = -0.90$ outside the chemical inhomogeneity and $H_{w3} = +0.90$ along the chemical inhomogeneity [i.e., from the sites $j = (M - b)/2 + 1$ to $j = (M + b)/2$, where b has also to be chosen as a (large) odd integer].

Note that both temperature T and boundary fields H_{w1}, H_{w2}, and H_{w3} are measured in units of the critical temperature T_{cb} of the bulk, i.e., [29] $k_B T_{cb}/J = 2/\ln(1 + \sqrt{2}) \approx 2.27$, where k_B is Boltzmann's constant and J the exchange constant, respectively. Thus, our Hamiltonian is

$$\mathcal{H} = -J \sum_{i=1}^{L} \sum_{j=1}^{M} S(i,j)[S(i+1,j)$$
$$+ S(i-1,j) + S(i,j+1) + S(i,j-1)]/2$$
$$- H_{w1} \sum_{j=1}^{M} S(L,j) - \sum_{j=1}^{M} H_w(j)S(1,j), \quad S(i,j) = \pm 1,$$
(1)

where $H_w(j) = H_{w2}$ for $1 \leqslant j \leqslant (M-b)/2$ and $(M+b)/2 + 1 \leqslant j \leqslant M$, while $H_w(j) = H_{w3}$ for $(M-b)/2 + 1 \leqslant$

$j \leqslant (M + b)/2$. $S(i,j) = 0$ is taken for missing neighbors.

Note that the chosen value of $H_{w3} = 0.90$ leads to a wetting critical temperature $t_w = T_w/T_{cb} \simeq 0.486\,6$ [31]. For this choice, the order within the bulk domains is almost perfect, and the correlation length in the bulk is of the order of the lattice spacing. Thus, also reduced temperatures $t = T/T_{cb}$ in the wet phase $t > t_w$ still can be varied over a significant range (where the interfacial tension changes already significantly) without entering the regime of critical fluctuations in the bulk, $1 - t \ll 1$. Note that typically we choose M much larger than b (e.g., $M = 303$ for $b = 51$) to make sure that there are no finite size effects associated with interfacial fluctuations. Also, note that typical extensions of the droplet in the y direction are only proportional to $\sqrt{b}$, and choosing L as large as at least $L = 120$ ensures that the droplet is not at all affected by the boundary at $i = L$, of course. To make it easier for the reader to establish the connection to fluid droplets, we will describe all our results in terms of local densities defined via $\rho(i,j) = (\langle S(i,j) \rangle + 1)/2$. Monte Carlo simulations were carried out with standard single spin-flip algorithms [36], carrying out runs typically with 2×10^7 Monte Carlo steps per site, starting with an initial condition where all spins are taken as $S(i,j) = -1$, in accord with the nonwet ground state of the system. Note that due to the presence of boundary fields and the fact that we do not work close to T_{cb}, cluster algorithms would not present any advantage [36].

III. NUMERICAL RESULTS

Figures 2–4 show typical density profiles for the case $L = 120$, $M = 303$, $b = 51$, and various choices of the reduced temperature t, focusing on either the density in the row $i = 1$ exposed to the surface field (Fig. 2) or perpendicular to the wall in the center of the droplet, i.e., $j = 152$ (Fig. 3). From Fig. 2 we see that even in the regime well above the wetting transition, the local density in the center of the droplet has not reached the density ρ_ℓ^{coex} of the liquid phase at coexistence (that is very close to the maximum value, $\rho_{max} = 1$). Also,
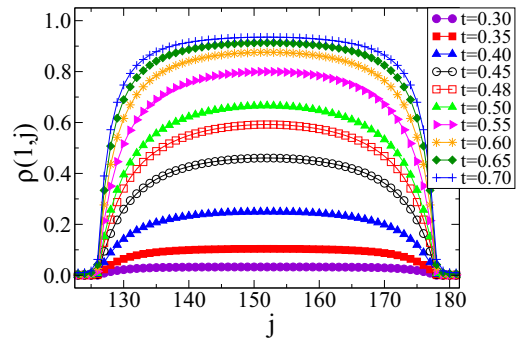
FIG. 2. Density profile $\rho(1,j)$ in the first row in which the surface fields H_{w2} and H_{w3} act, for the case $L = 120$, $M = 303$, and $b = 51$, for various temperatures t both below and above the wetting transition, as indicated in the key to the figure. In this case the positive surface field (which favors the liquid) ranges from $j = 127$ to $j = 177$. Note that the statistical errors of the simulation data points in this figure and the following figures typically are smaller than the size of the symbols and therefore are not shown.
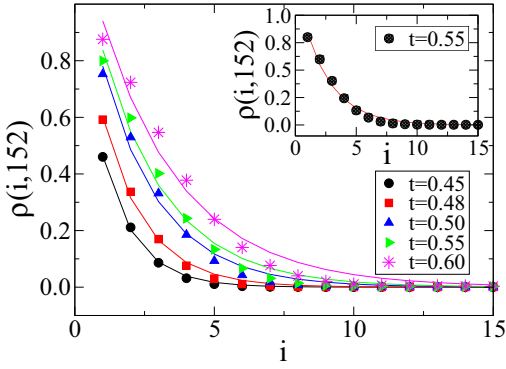
FIG. 3. Density profile $\rho(i,152)$ plotted vs i for the same system as shown in Fig. 2, showing several temperatures, both below and above the wetting transition. The insert shows, as an example, a fit of the data to Eq. (2) at $t = 0.55$, with parameters $A_0 = 0.84$ and $\xi_\perp = 2.36$.

the local maximum (in the center of the droplet, $j = 152$ in this case) is approached as a function of j very slowly. Furthermore, the regime to the left site $j = 127$, where the chemical heterogeneity of the substrate starts, and the regime to the right of the site $j = 177$, where it ends, are hardly affected, and $\rho(1,j)$ stays very small. Figure 3 also shows that the wetting film that is stabilized in between $j = 127$ and $j = 177$ only is a few lattice spacings thick. We can fit the decay of the density with the distance from the surface by a simple exponential decay,

$$\rho[j = (M+1)/2, i] = A_0 \exp[-x/\xi_\perp(b,t)], \qquad (2)$$

where we have neglected the small background density of the gas phase at large distances x ($x = i$, when distances are measured in units of the lattice spacing). The length $\xi_\perp(b,t)$ extracted from the fit will be discussed further below, here we also note that similar fits can be performed for other values of j in the region of the chemical inhomogeneity as well (Fig. 4). As has already been discussed in detail in the literature [14,34,38,40,41], it can be shown that the shape of a droplet attached to a chemical inhomogeneity of extent b in the regime of complete wetting of this inhomogeneity has the shape of a semiellipse (as qualitatively shown on the inset of Fig. 4), with
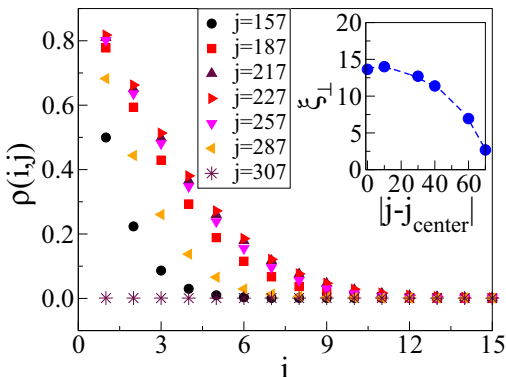
FIG. 4. Density profiles $\rho(i,j)$ for the case $L = 300$, $M = 453$, and $t = 0.50$ plotted vs i, showing various choices of j. Note that here the droplet center occurs at $j_{center} = 227$. The inset shows the correlation length $\xi_\perp$ as a function of $|j - j_{center}|$.
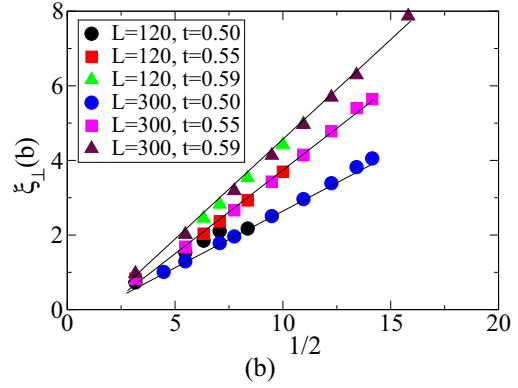
FIG. 5. Plot of the length scale $\xi_\perp(b)$ vs $b^{1/2}$ as evaluated for $t = 0.50, 0.55$, and 0.59, including two choices of L to show that the systematic dependence on L is negligible. Full lines are drawn to guide the edge only.

the small axis of the ellipse scaling as $b^{1/2}$ as $b \to \infty$. Figure 5 gives an example where $\xi_\perp(b,t)$ in the wet regime is plotted vs $b^{1/2}$; evidence for the expected scaling $\xi_\perp(b,t) \propto b^{1/2}$ is readily obtained. Of course, we do not expect that Eq. (2) is an exact description for all values of x and all the cases studied, and hence it is difficult to quote precise errors for the fitted values of this transverse correlation length. We expect that the errors of this correlation length typically will be of the order of a few percent.

It also is interesting to study the variation of the density distribution of ρ varying b right at the wetting transition temperature [Fig. 6(a)]. Also, for $T = T_w$ a scaling of the approach of the data to the limiting behavior for $b \to \infty$ with $b^{-1/2}$ is observed [Fig. 6(b)], and for b large enough there works a superposition principle approximately [Fig. 6(c)]. This is clearly not the case for $T < T_w$, where the profiles develop a horizontal region at the top, showing a saturation at a value ρ_{max} far from the density of the bulk liquid phase [Fig. 7(a)]. In contrast, for $T > T_w$ the behavior is qualitatively similar to the behavior at $T = T_w$ [Fig. 7(c)]. But rather nontrivial shapes of the density profile are obtained when one varies the distance i from the surface [Fig. 7(d)].

Next we consider the scaling of the behavior of the droplet formation as we approach the wetting transition from below [Fig. 8(a)]. For T far below T_w, the maximum density ρ_{max} in the center of the droplet reaches a maximum value that is rather small, and this maximum value is reached for $b > b^*(t)$, where $b^*(t)$ is some characteristic crossover length of the chemical inhomogeneity. For practical purposes, $b^*(t)$ is determined from the intersection between the initial slope and the plateau line in plots such as those shown in Fig. 8(a). As one approaches t_w, ρ_{max} increases and also the approach towards the plateau with increasing b becomes very slow. As Fig. 8(b) demonstrates, the estimation of $\rho_{max}(t)$ is still possible for the shown data for $t \leqslant 0.40$, but already for $t = 0.42$ the extrapolation towards $b^{-1/2} \to 0$ already is very questionable, and for $t = 0.45$ it is clearly impossible: considerably larger values to b (and hence M) would be required.

In Fig. 9 we study the behavior shown in Fig. 8 more closely, focusing on the temperature dependence of $\rho_{max}(t)$
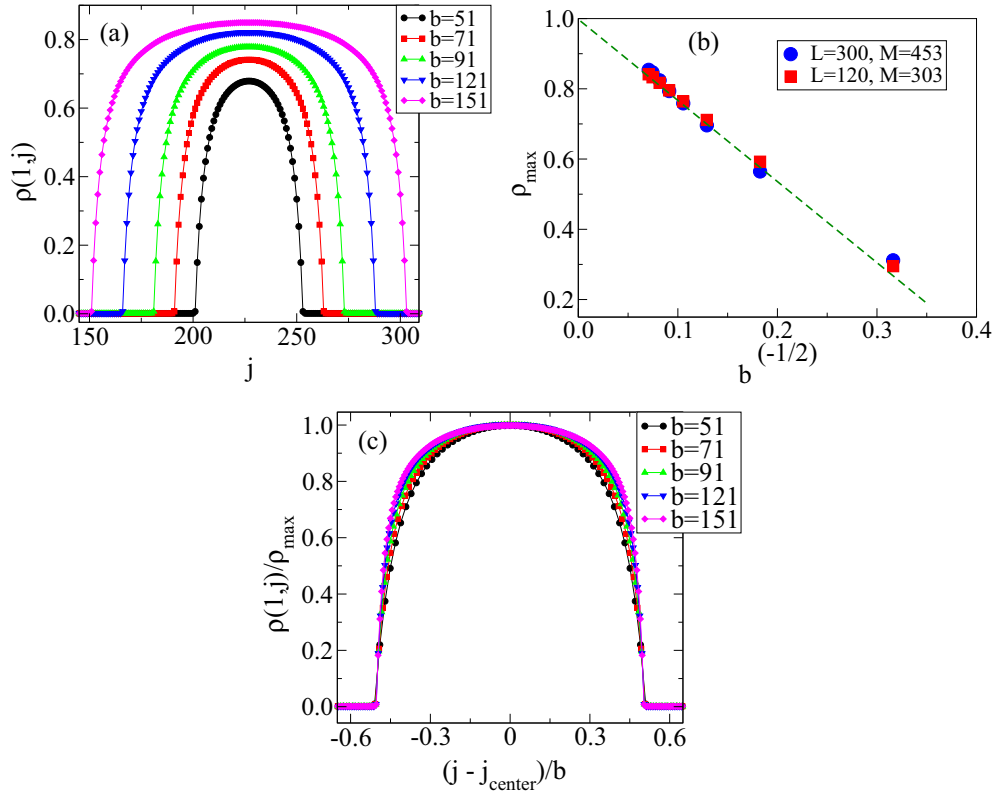
FIG. 6. (a) Plot of $\rho(1,j)$ vs j for a system at $t = t_w = 0.486\,6$ for $L = 300$, $M = 453$, and various choices of b, as shown in the key. (b) Plot of the maximum density $\rho_{max} = \rho[1, j = (M+1)/2]$ of the data in part (a) versus $b^{-1/2}$. Note that for $b \to \infty$ ρ_{max} differs from unity only by a deviation of about 0.001 15, invisible at the scale of this plot. (c) Plot of the normalized density profile $\rho(1,j)/\rho_{max}$ vs the normalized distance from the center of the droplet ($j_{center} = \frac{M+1}{2}$), $x_{norm} = (j - j_{center})/b$, for the data of Fig. 6(a).
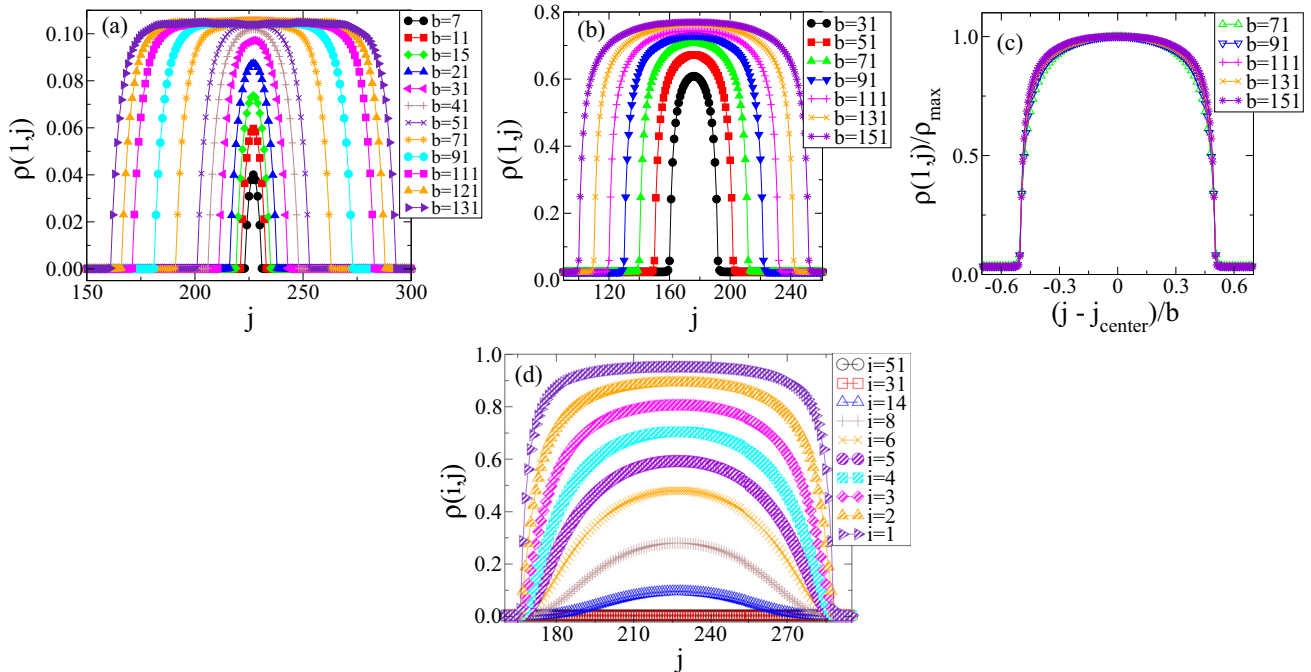
FIG. 7. (a) Plot of $\rho(1,j)$ vs j for a system at $t = 0.35$ for $L = 300$, $M = 453$, and different values of b as indicated. (b) Plot of $\rho(1,j)$ vs j for a system at $t = 0.60$, i.e., in the regime of complete wetting, for $L = 300$, $M = 453$, and different values of b, as indicated. (c) Plot of the normalized density profile $\rho(1,j)/\rho_{max}$ vs the normalized distance from the center of the droplet ($j_{center} = \frac{M+1}{2}$), $x_{norm} = (j - j_{center})/b$, for the data of Fig. 7(b). (d) Plot of $\rho(i,j)$ vs j for a system at $t = 0.60$, $L = 300$, $M = 453$, and $b = 121$, showing density profiles for various choices of i, as indicated.
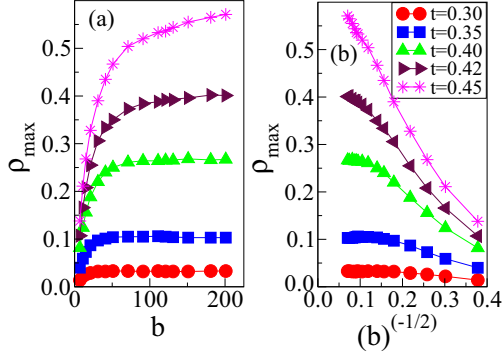
FIG. 8. Plot of the maximum density $\rho_{\max}(t)$ of the droplet, measured at the center of the inhomogeneity, i.e. $\rho_{\max}(t) = \rho(1, j = (M+1)/2)$, versus (a) b and (b) $b^{-1/2}$, as obtained for different values of temperature T taken below T_w. All data correspond to $L = 300$ and $M = 453$. Note that for large enough b for all temperatures $T < T_w$ a saturation at a value $\rho_{\max}(t) < \rho_\ell^{\mathrm{coex}}(t)$ occurs, if b exceeds a characteristic value b^* (see text).

[Fig. 9(a)] and on the scaling behavior of the approach to saturation [Fig. 9(b)]. Of course, reduced temperatures such as $t = 0.30$ and $t = 0.35$ are rather remote from t_w, and hence systematic deviations from scaling clearly are obvious.

It is clear that the behavior seen in Figs. 8 and 9 is due to the critical fluctuations associated with the critical wetting transition at $t = t_w$, and this fact becomes even more obvious when we study the transverse correlation length $\xi_\perp(b,t)$ that we may extract from Eq. (2), as discussed earlier (see Fig. 10). The temperature dependence $\xi_\perp(b \to \infty, t) \propto (t_w - t)^{-1}$ found in Fig. 10(c), confirms our expectation that the length $\xi_\perp(b \to \infty, t)$ extracted from Eq. (2) near $t = t_w$ is simply proportional to the transverse correlation length of a (weakly bound) linear interface near the boundary of a semi-infinite system close to the wetting transition. Thus, it is tempting to assume that on the nonwet side of the wetting transition, but rather close to it, all distances describing the variation of the local density $\rho(i, \Delta j, b, t)$, where $\Delta j = j - (M+1)/2$ and $M \to \infty$ is taken, should be scaled with the appropriate correlation lengths $\xi_\parallel(t) \propto (t_w - t)^{-2}, \xi_\perp(t) \propto (t_w - t)^{-1}$ [32]
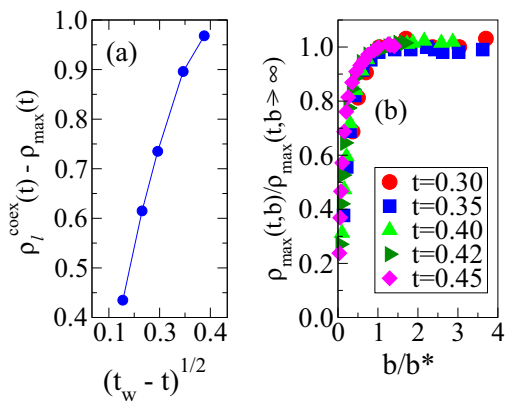
FIG. 9. (a) Plot of $\rho_\ell^{\mathrm{coex}}(t) - \rho_{\max}(t)$ versus $(t_w - t)^{1/2}$. (b) Plot of $\rho_{\max}(t,b)/\rho_{\max}(t, b \to \infty)$ vs b/b^*. Several values of t are used, as indicated.
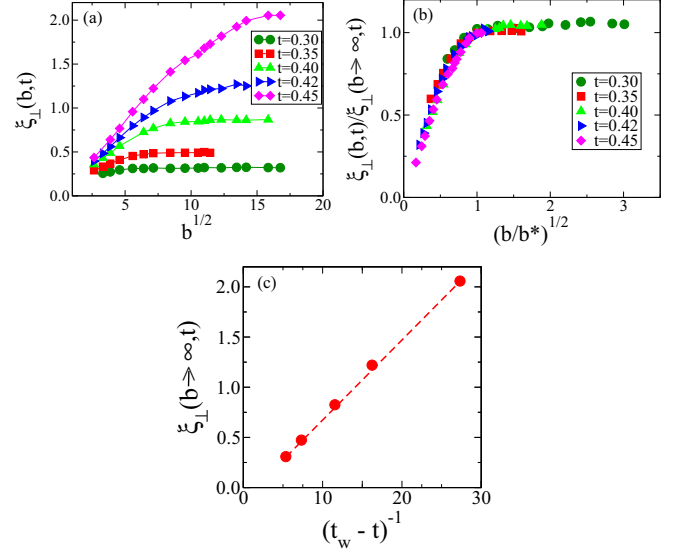
FIG. 10. (a) Plot of the transverse correlation length $\xi_\perp(b,t)$, as defined from the fit of $\rho[i, j = (M+1)/2]$ according to Eq. (2), versus $b^{1/2}$ and several choices of t, as specified in the key to part (b). (b) Plot of $\xi_\perp(b,t)/\xi_\perp(b \to \infty, t)$ versus $(b/b^*)^{1/2}$. Note that both scaling parameters b^* and $\xi_\perp(b \to \infty, t)$ were obtained by optimizing the data collapse on a common master curve. All data refer to the choice $L = 300$, $M = 453$. (c) Plot of $\xi_\perp(b \to \infty, t)$ versus $(t_w - t)^{-1}$.

of the critical wetting transition,

$$\rho(i, \Delta j, b, t) - \rho_{\mathrm{vapor}}^{\mathrm{coex}}(t) = \tilde{\rho}\left(\frac{i}{\xi_\perp(t)}, \frac{\Delta j}{\xi_\parallel(t)}, \frac{b}{\xi_\parallel(t)}\right), \quad (3)$$

where $\tilde{\rho}$ is a corresponding scaling function. The scaling behavior seen in the above figures clearly can all be deduced from such a general scaling assumption. Right at $t = t_w$, when $\xi_\parallel(t)$ and $\xi_\perp(t)$ diverge, one can eliminate one of these scaling variables [note $\xi_\perp(t) \propto [\xi_\parallel(t)]^{1/2}$] to find

$$\rho_w(i, \Delta j, b) - \rho_{\mathrm{vapor}}^{\mathrm{coex}}(t_w) = \tilde{\rho}_w\left(\frac{i}{b^{1/2}}, \frac{\Delta j}{b}\right), \quad t = t_w. \quad (4)$$

To investigate Eq. (4) more closely, the full distribution $\rho_w(i, \Delta j, b)$ has been recorded (Fig. 11). Since the required statistical effort due to the critical slowing down associated with the critical wetting transition is quite large (15×10^6 Monte Carlo steps per spin were used in Fig. 11), no attempt was made to test the scaling description of Eq. (4) in terms of two scaling variables fully. But at least one can verify nicely that the total density excess associated with the droplet shows the expected scaling behavior [we symbolically replace here summations over $i, \Delta j$ by integrations over continuous x, y coordinates]

$$\Delta \rho = \int dx\, dy\, [\rho_w(x, y, b) - \rho_{\mathrm{vapor}}^{\mathrm{coex}}(t_w)] \propto b^{3/2}, \quad (5)$$

which is implied in the semielliptical shape of having a droplet of small axis proportional to $b^{1/2}$ if the long axis is b.

In Figs. 12(a) and 12(b) we study the variation of $\Delta \rho$ [cf. Eq. (5)] with b, both for $T < T_w$ [Fig. 12(a)] and for $T > T_w$ [Fig. 12(b)]. In the latter case, clear evidence for a
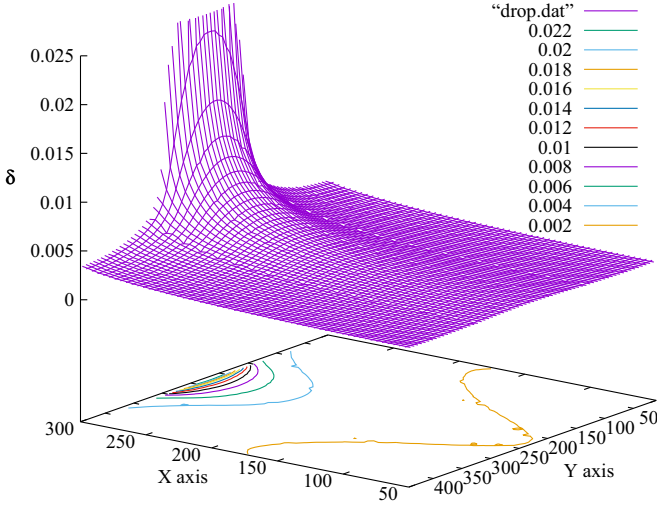
FIG. 11. Plot of the averaged density $\delta(i,j,b) \equiv LM\rho(i,j,b)$ vs $i \equiv X$ and $\Delta j \equiv Y$ measured at $T = T_w$, for the choice $L = 300$, $M = 453$, and $b = 151$. In addition to the three-dimensional plot, also the equal-density curves projected into the (X,Y) plane are shown. Note that density values at the plane $X = 300$ are underestimated due to the coarse graining algorithm used for the $3d$ plot.

$b^{3/2}$ law is found, as expected [38,40]. Note, however, that we do not study here the crossover in the droplet shape from semielliptical droplets to semispherical ones, when the length
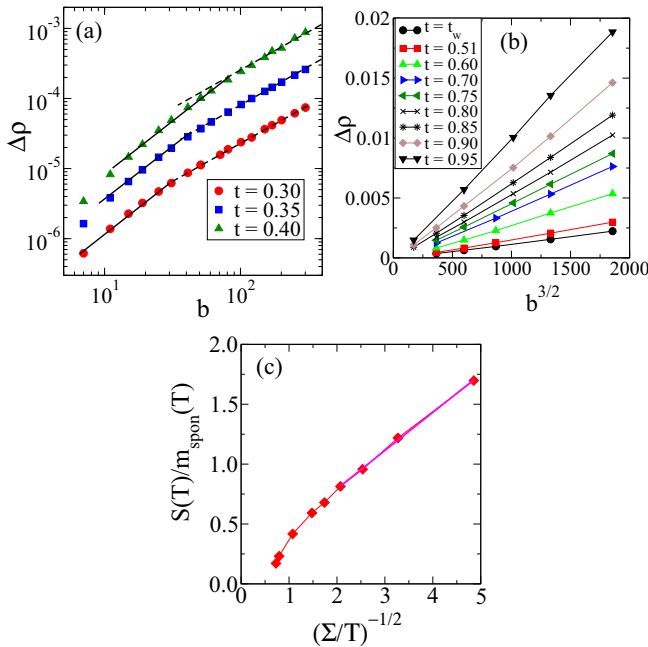
FIG. 12. (a) Log-log plot of the total density excess $\Delta\rho$ plotted vs b for three choices of t, as indicated. Full straight lines indicate a slope of 3/2, while broken straight lines indicate a slope of 1. (b) Plot of $\Delta\rho$ vs $b^{3/2}$ at temperatures $t = t_w = 0.4866$ as well as $t > t_w$, as indicated. (c) Slopes of the straight lines in part (b), [$S(T)$] normalized by the spontaneous magnetization $m_{\rm spon}(T)$ plotted vs $(\Sigma/T)^{-1/2}$, where Σ is the interfacial stiffness known from the exact solution [Eq. (9)] [44]. The leftmost symbol shown corresponds to $t = t_w = 0.4866$ and the rightmost to $t = 0.95$. The straight line has slope 0.3185 and shows the best fit of the data for $t \geqslant 0.80$.

b is comparable to the correlation length in the bulk. Right at bulk criticality, a semicircular droplet shape has been found [41].

For $T < T_w$, on the other hand [cf. Fig. 12(a)], we observe a crossover from a $b^{3/2}$ law at small b to a behavior linear in b at large values of b. For $t = 0.30$, this crossover occurs at about $b_c \approx 30$, at $t = 0.35$ at about $b_c \approx 52$, and at $t = 0.40$ at about $b_c \approx 83$. Roughly speaking, we would expect such a crossover when $b/2 = \xi_{||}(t)$, the correlation length associated with critical wetting in the direction parallel to the boundary from which the interface unbinds. Of course, the chosen temperatures are clearly not close enough to $t = t_w$, where the power law $\xi_{||}(t) \propto (t_w - t)^{-\nu_{||}}$ with $\nu_{||} = 2$ would hold. For $b < b_c$ we have essentially a single droplet bound to the "wall," while for $b \gg b_c$ there occurs a liquid precursor film of thickness $\xi_\perp(t)$ in the region from $j = (M - b)/2 + 1$ to $j = (M + b)/2$, where the positive surface field acts. As is well known [34], this liquid film in the partially wet region which is a precursor of the wetting film that exists for $t > t_w$ when the interface has become detached from the "wall" does not have a uniform thickness but rather can be viewed as a sequence of droplets; these droplets have a lateral size of order $\xi_{||}(t)$ and a vertical size of order $\xi_\perp(t)$, and $\xi_{||}(t) \propto \xi_\perp^2(t)$, so that for $b_c = 2\xi_{||}(t)$ a smooth crossover to a single droplet of semielliptical shape can occur.

This problem of the temperature dependence of the droplet shape of a wall-attached droplet has been studied previously in the framework of the solid-on-solid model [40–43]. Burkhardt [40] suggested that the typical droplet shape can be described by an ellipse of the form

$$x^2 + \frac{K}{c}\frac{b}{2}y^2 = (b/2)^2, \qquad (6)$$

where K is a constant of order unity (which can be related to the inverse temperature J/T of the Ising model), and the constant $c = 1/\sqrt{\pi} = 0.5642$ for the average shape at $T = T_w$, while for $T > T_w$ a crossover to a larger value $2/\sqrt{\pi}$ occurs, in a region of order unity in the crossover scaling variable $b/\xi_{||}$. Similarly, for $T < T_w$, a crossover scaling to $c = 0$ occurs also when $b/\xi_{||}$ is of order unity. This behavior is qualitatively compatible with our findings. Note, however, that in the SOS model the bulk critical temperature $T_{cb}^{\rm SOS} \to \infty$; hence this model does not exhibit a reasonable temperature dependence for the interfacial free energy, as it occurs in the Ising model.

Jakubczyk *et al.* [42,43] have generalized this SOS model approach in terms of an interface Hamiltonian approach, addressing the problem in terms of a continuum variable $\ell(x)$ describing the distance of the interface between the liquid phase (at density $\rho_\ell^{\rm coex}$) and the vapor phase (at density $\rho_v^{\rm coex}$) from the wall,

$$\mathcal{H}[\ell(x)] = \int_{-M/2}^{+M/2} dx \left[\frac{\Sigma(T)}{2}\left(\frac{d\ell}{dx}\right)^2 + V(x,\ell) \right], \qquad (7)$$

where $\Sigma(T)$ is the interfacial stiffness, the potential $V(x,\ell)$ was taken piecewise constant, with one value for $|x| \leqslant b$ and another one for $b < |x| \leqslant M/2$, and $\mathcal{H}$ is already normalized by T. From this treatment one finds the small axis of the ellipse to be $\sqrt{b/[2\pi\,\Sigma(T)]}$ in the regime of complete wetting, and

hence the area then scales as

$$\Delta\rho = \left(\rho_\ell^{\text{coex}} - \rho_v^{\text{coex}}\right)\tfrac{1}{4}b^{3/2}\sqrt{\pi/2\Sigma(T)}. \qquad (8)$$

Figure 12(b) shows plots of $\Delta\rho$ vs $b^{3/2}$ as obtained at the wetting temperature as well as within the complete wetting regime. The obtained straight lines and the temperature-dependent slopes [$S(T)$] suggest that Eq. (8) holds. In fact, for a deeper understanding we note that near the bulk critical temperature the interfacial stiffness [44]

$$\Sigma(T) = \sinh\{2J/T - \ln[\coth(J/T)]\} \qquad (9)$$

agrees with the interfacial free energy of the Ising ferromagnet [44], and hence $\Delta\rho \propto (1-t)^{-(\frac{\nu}{2}-\beta)} = (1-t)^{-3/8}$, when $t = T/T_{cb} \to 1$, where we used the Ising model critical exponents for order parameter and interfacial free energy given by the following relationships: $\rho_\ell^{\text{coex}} - \rho_v^{\text{coex}} \propto (1-t)^\beta = (1-t)^{1/8}, \sigma(T) \propto (1-t)^\nu = 1-t$, respectively. This critical behavior implicit in Eq. (8) is not compatible with the findings of Burkhardt [40], which are only useful very close to the wetting transition, while Eq. (8) does not describe the behavior close to that transition. Of course, near bulk criticality also crossovers involving the bulk correlation length $\xi_b \propto (1-t)^{-\nu}$ will come into play, which we have not attempted to address. On the other hand, Fig. 12(c) shows plots of $S(T)/m_{\text{spon}}$ vs $[\Sigma(T)/T]^{-1/2}$, as suggested by Eq. (8), where m_{spon} is the spontaneous magnetization of the Ising ferromagnet [30]. The obtained slope in the high-temperature regime ($t = T/T_{cb} \to 1$), given by $s = 0.3185$ agrees with the theoretical calculation, namely, $s = \tfrac{1}{4}\sqrt{\pi/2} \simeq 0.31333$, cf. Eq. (8). Thus, although the problem of droplets in the $d = 2$ Ising/lattice gas model attached to a wall has been considered for a long time with various methods, there still seems to be the need for further work in order to obtain a unified description within the range $t_w \leqslant t \leqslant t_{cb}$.

IV. CONCLUSION

In this work we have presented a Monte Carlo simulation study of liquid adsorption on a structured substrate within the framework of the two-dimensional Ising model, where the substrate inhomogeneity is described by a positive boundary field applied over a distance of b lattice sites, while outside this region a negative boundary field acts such that in the bulk

of the system the vapor phase is stabilized. Consistent with previous predictions based on SOS model treatments, we have found that near the wetting transition adsorption starts right at the inhomogeneity of the boundary field, and one has to proceed away from this inhomogeneity over a distance $\xi_{||}(t)$, where $\xi_{||}(t)$ is the correlation length associated with the wetting transition, describing the correlation of interface fluctuations in the direction parallel to the substrate, to reach a region where the fluid density is constant. At the wetting transition, the density distribution stays inhomogeneous over the whole range of the inhomogeneity (b), and the perpendicular direction there is always an exponential decay of the density distribution, described by a correlation length $\xi_\perp(t) \propto [\xi_{||}(t)]^{1/2}$ (or by $b^{1/2}$, in the regime where the correlation length $\xi_{||}(t)$ would exceed the range b of the inhomogeneity). Also in the regime of complete wetting, this droplet extension in perpendicular direction stays of order $b^{1/2}$ throughout, and we have found that in this regime then the total adsorbed amount scales like $b^{3/2}$. The prefactor in this relation exhibits an interesting temperature dependence as well as crossover phenomena both near the bulk critical temperature and near the wetting transition, respectively. Our numerical Monte Carlo results describe correctly the behavior of the adsorbed fluid on the inhomogeneous substrate close to both critical wetting (theoretically described by means of a SOS approach [40–43]) and in the regime of complete wetting (theoretically addressed by means of an interfacial Hamiltonian approach [42,43]). So, the development of a unified theoretical treatment capable to account for both regimes has not yet been fully explored and will certainly be welcomed.

[1] *Handbook of Nanophysics, Principles and Methods*, edited by K. D. Sattler (CRC Press, Boca Raton, FL, 2011).

[2] *Nanoscale Liquid Interfaces: Wetting, Patterning, and Force Microscopy at the Molecular Scale*, edited by Th. Ondarçuhu and J.-P. Aimé (Pan Stanford Publishing, Singapore, 2013).

[3] M. Rauscher and S. Dietrich, Annu. Rev. Mater. Res. **38**, 143 (2008).

[4] M. Rauscher and S. Dietrich, in *Handbook of Nanophysics, Principles and Methods*, edited by K. D. Sattler (CRC Press, Boca Raton, FL, 2011), Chap. 11.

[5] S. Dietrich, M. Rauscher, and M. Napiorkowski, in *Nanoscale Liquid Interfaces: Wetting, Patterning, and Force Microscopy at the Molecular Scale*, edited by Th. Ondarçuhu and J.-P. Aimé (Pan Stanford Publishing, Singapore, 2013), Chap. 3.

[6] W. Koch, S. Dietrich, and Napiorkowski, Phys. Rev. E **51**, 3300 (1995).

[7] Th. Ondarçuhu, J. Phys. II (France) **5**, 227 (1995).

[8] H. Gau, S. Herminghaus, P. Lenz, and R. Lipowsky, Science **283**, 46 (1999).

[9] C. Bauer, S. Dietrich, and A. O. Parry, Europhys. Lett. **47**, 474 (1999).

[10] C. Bauer and S. Dietrich, Phys. Rev. E **60**, 6919 (1999).

[11] C. Bauer and S. Dietrich, Eur. Phys. J. B **10**, 767 (1999).

[12] P. Lenz and R. Lipowsky, Eur. Phys. J. E: Soft Matter Biol. Phys. **1**, 249 (2000).

[13] R. Lipowsky, Interface Sci. **9**, 105 (2001).

[14] A. O. Parry, E. D. Macdonald, and C. Rascon, J. Phys.: Condens. Matter **13**, 383 (2001).

[15] M. Brinkmann and R. Lipowsky, J. Appl. Phys. **92**, 4296 (2002).

[16] F. Jakubczyk and M. Napiorkowski, J. Phys.: Condens. Matter **16**, 6917 (2004).

[17] S. Mechkov, M. Rauscher, and S. Dietrich, Phys. Rev. E **77**, 061605 (2008).

[18] J. W. Gibbs, in *The Collected Works of J. Willard Gibbs* (Yale University Press, London, 1957), p. 288.

[19] J. S. Rowlinson and B. Widom, *Molecular Theory of Capillarity* (Clarendon Press, Oxford, 1982).

[20] J. Gaydos and A. W. Neumann, J. Colloid Interface Sci. **120**, 76 (1987).

[21] J. O. Indekeu, Int. J. Mod. Phys. B **8**, 309 (1994).

[22] J. Drelich, Colloids Surf. A **116**, 43 (1996).

[23] T. Getta and S. Dietrich, Phys. Rev. E **57**, 655 (1998).

[24] J. Y. Wang, S. Betelu, and B. M. Law, Phys. Rev. Lett. **83**, 3677 (1999).

[25] T. Pompe, Phys. Rev. Lett. **89**, 076102 (2002).

[26] D. Gandolfo, L. Laanait, S. Miracle-Sole, and J. Ruiz, J. Stat. Phys. **126**, 133 (2006).

[27] L. Schimmele, N. Napiorkowski, and S. Dietrich, J. Chem. Phys. **127**, 164715 (2007).

[28] S. Sefiane, Eur. Phys. J. Spec. Top. **197**, 151 (2011).

[29] L. Onsager, Phys. Rev. **65**, 117 (1944).

[30] C. N. Yang, Phys. Rev. **85**, 808 (1952).

[31] D. B. Abraham, Phys. Rev. Lett. **44**, 1165 (1980).

[32] D. B. Abraham, in *Phase Transitions and Critical Phenomena*, edited by C. Domb and J. L. Lebowitz (Academic Press, London, 1986), Vol. 18, Chap. 1.

[33] D. B. Abraham, J. De Coninck, and F. Dunlop, Phys. Rev. B **39**, 4708 (1989).

[34] M. E. Fisher, J. Stat. Phys. **34**, 667 (1984).

[35] X.-T. Wu, D. B. Abraham, and J. O. Indekeu, Phys. Rev. Lett. **116**, 046101 (2016).

[36] K. Binder and D. W. Heermann, *Monte Carlo Simulation in Statistical Physics, An Introduction*, 5th ed. (Springer, Berlin, 2010).

[37] K. Binder and D. Stauffer, J. Stat. Phys. **6**, 49 (1972).

[38] W. Selke, J. Stat. Phys. **56**, 609 (1989).

[39] A. Checco, O. Gang, and B. M. Ocko, Phys. Rev. Lett. **96**, 056104 (2006); A. Checco and B. M. Ocko, Phys. Rev. E **77**, 061601 (2008).

[40] T. W. Burkhardt, Phys. Rev. B **40**, 6987 (1989).

[41] T. W. Burkhardt, W. Selke, and T. Xue, J. Phys. A: Math. Gen. **22**, L1129 (1989).

[42] P. Jakubczyk, M. Napiorkowski, and A. O. Parry, Phys. Rev. E **74**, 031608 (2006).

[43] P. Jakubczyk and M. Napiorkowski, J. Phys. A: Math. Theor. **40**, 2363 (2007).

[44] M. P. A. Fisher, D. S. Fisher, and J. D. Weeks, Phys. Rev. Lett. **48**, 368 (1982).